J. Fluid Mech. (1997), *vol.* 348, *pp.* 177–199. Printed in the United Kingdom

Orthonormal wavelet decomposition of turbulent flows: intermittency and coherent structures

By R. CAMUSSI AND G. GUJ

Università degli studi 'Roma Tre' Dipartimento di Ingegneria Meccanica ed Industriale, via C. Segre no 60, 00146 Roma, Italy

(Received 6 August 1996 and in revised form 13 May 1997)

Experimental data obtained in various turbulent flows are analysed by means of orthogonal wavelet transforms. Several configurations are analysed: homogeneous grid turbulence at low and very low Re_λ, and fully developed jet turbulence at moderate and high Re_λ. It is shown by means of the wavelet decomposition in combination with the form of scaling named extended self-similarity that some statistical properties of fully developed turbulence may be extended to low-Re_λ flows. Indeed, *universal* properties related to intermittency are observed down to $Re_\lambda \simeq 10$. Furthermore, the use of a new conditional averaging technique of velocity signals, based on the wavelet transform, permits the identification of the time signatures of coherent structures which may or may not be responsible for intermittency depending on the scale of the structure itself. It is shown that in grid turbulence, intermittency at the smallest scales is related to structures with small characteristic size and with a shape that may be related to the passage of vortex tubes. In jet turbulence, the longitudinal velocity component reveals that intermittency may be induced by structures with a size of the order of the integral length. This effect is interpreted as the signature of the characteristic jet mixing layer structures. The structures identified on the transverse velocity component of the jet case turn out on the other hand not to be affected by the mixing layer and the corresponding shape is again correlated with the signature of vortex tubes.

1. Introduction

In 1941 Kolmogorov laid the foundations of the statistical theory of homogeneous and isotropic turbulence at high Reynolds number (hereafter referred to as the K41 theory). By means of simple dimensional analyses, Kolmogorov (1941) obtained the following scaling law of the so-called p-order velocity structure function (see e.g. Monin & Yaglom 1975):

$$\langle \Delta V(r)^p \rangle = \langle [V(x+r) - V(x)]^p \rangle \sim r^{\zeta(p)}, \tag{1.1}$$

with $\zeta(p) = p/3$. In terms of wavenumbers $k = 2\pi f/\overline{V}$, where f represents the frequency and $\overline{V}$ the mean velocity, the well-known $E(k) \sim k^{-5/3}$ law applies for the energy-spectrum $E(k)$. As pointed out by Vassilicos (1996), a non-integer value of the scaling exponent of the energy spectrum corresponds to the effect of *singularities* in the turbulent flow that physically may be correlated with the presence of coherent structures.

Several experiments and numerical simulations (e.g. Batchelor & Townsend 1949;

Anselmet *et al.* 1984; Meneveau & Sreenivasan 1991; Vincent & Meneguzzi 1992; Briscolini & Santangelo 1994) have shown that the K41 theory is not completely correct in the sense that the scaling law (1.1) is affected by the intermittent nature of the turbulent energy rate of dissipation, ϵ, which, in Cartesian coordinates, is defined as (Hinze 1975)

$$\epsilon = \nu \left(\frac{\partial V_i}{\partial x_j} + \frac{\partial V_j}{\partial x_i} \right)^2, \tag{1.2}$$

where ν is the kinematic viscosity. Intermittency is then related to the presence of rare but strong velocity gradients that are generated by highly coherent structures (see also She, Jackson & Orszag 1991). In contrast with the K41 idea, intermittency yields the important consequence that the flow *singularities*, that represents the highly coherent structures, are not *space filling* (see Meneveau & Sreenivasan 1991). From a practical point of view, the presence of intermittency may be evaluated by the nonlinear dependence of $\zeta(p)$ over p. This behaviour may be related to the non-Gaussianity of the probability distribution functions (PDF) of the velocity difference field (e.g. Kolmogorov 1962; Oboukov 1962; Castaing, Gagne & Hopfinger 1990; She 1991) whose tails move closer to exponential functions as the separation scale becomes smaller.

The connection between coherent structures and intermittency in fully developed turbulence has motivated several numerical analyses (e.g. Kerr 1985; She *et al.* 1991; Jiménez *et al.* 1993) due to the importance that this aspect has for turbulence modelling and flow control problems. In particular, numerical simulations have demonstrated the presence of *worm-like* structures even in homogeneous and isotropic turbulence, but the role and the actual shape of such structures in real turbulent flows is not fully understood. Filamentary structures are also the basis of a recent model (She & Levesque 1994), which predicts scaling exponents in good agreement with experimental results (e.g. those of Benzi *et al.* 1993*b*). The presence of filamentary structures in isotropic and homogeneous turbulence seems to be confirmed also by some experimental investigations (e.g. Kuo & Corrsin 1972; Douady & Coudet 1991; Cadot, Douady & Coudet 1995; Villermeaux & Brachet 1995). These experiments have been performed for moderate $Re_\lambda = \sigma_V \lambda / \nu$ (where λ is the Taylor microscale and σ_V the r.m.s. longitudinal velocity) homogeneous isotropic flows ($Re_\lambda \geqslant 100$). Nevertheless, the relation between coherent structures and intermittency inside the dissipation range (or for very low Re_λ) has not yet been extensively studied. In summary, the nature and shape of coherent structures in homogeneous isotropic turbulence, their relation with the observed scaling laws and PDF shape, and their importance in the dissipation range, are still open questions and are the principal aspects that have motivated the present work.

In the present paper, the connection between coherent structures and intermittency is studied by a proper analysis of velocity signals obtained from hot-wire measurements using single and double probes. Velocity signals obtained in grid and jet turbulence for Re_λ ranging from 3 to 800 are processed by using the combined application of wavelet transform (Meneveau 1991*a*) with the extended self-similarity (ESS) form of scaling (Benzi *et al.* 1993*a*, *b*). This approach permits the analysis of intermittency properties and, in this case, particular emphasis is given to the low-Re_λ cases. Secondly, the wavelet decomposition is used for constructing a coherent-structures identification technique. The methodology is based on the idea that even homogeneous and isotropic turbulence is characterized by the presence of coherent structures which are intermittent and lead to an intermittent energy distribution at the smallest scales.

This behaviour is related to the presence of strong velocity gradients which characterize the passage of highly coherent vortical structures. Owing to the intermittent nature and to the singular shape of such structures, wavelet transform decomposition appears as an optimal tool for their eduction. The identification technique is applied first to an artificial signal for validation, and then to real turbulence data thereby allowing vortex structures to be clearly identified.

In the next section the main characteristics of wavelet transforms are presented. In § 3 the new procedure for the conditional averages of velocity signals is presented and tested on a properly generated *artificial* signal. Subsequently (§ 4), the ESS form of scaling is briefly explained. Flow conditions are summarized in § 5 and in § 6 principal results are presented and discussed.

2. Orthogonal wavelet transform

The need of a time–frequency signal representation (or space–wavenumbers if the Taylor hypothesis is adopted), which is necessary for analysing turbulent structures with intermittent nature, has lead us to use the wavelet transform. The wavelet decomposition of turbulent signals is a recent technique which has received considerable attention in the last few years. Extensive reviews of the wavelet decomposition technique can be found e.g. in Farge (1992) and Daubechies (1992) (see also the references therein). In the present work, discrete one-dimensional orthonormal wavelets are used. This choice has been dictated mainly by the non-redundancy of the corresponding wavelet coefficients. This property may be particularly useful when dealing with a large number of samples, as in the present case. Accurate reviews of properties and advantages of such a decomposition are given also in Mallat (1989) and Meneveau (1991*a*).

The wavelet transform of a signal $V(x)$ at a scale r at the position x, is defined as (Farge 1992)

$$w(r,x) = C_\Psi^{-1/2} r^{-1/2} \int_\infty^\infty \Psi^* \left(\frac{y-x}{r}\right) V(y)\mathrm{d}y, \tag{2.1}$$

where $\Psi(x)$ is the function called a wavelet, which satisfies the following so-called admissibility condition:

$$C_\Psi = \int_\infty^\infty |k|^{-1} |\hat{\Psi}(k)|^2 \mathrm{d}k < \infty, \tag{2.2}$$

with $\hat{\Psi}(k)$ denoting the Fourier transform of $\Psi(x)$. Equation (2.2) is the invertibility condition (e.g. Farge 1992) which is a necessary condition for the signal $V(x)$ to be reconstructable from its wavelet coefficients. The wavelet transform may be considered as the total contribution of $V(x)$ at the scale r at x. An important property of the wavelet transform (see also Arneodo, Grasseau & Holshneider 1988; Bacry *et al.* 1989; Farge 1992; Mimouni *et al.* 1995) is that, if $V(x)$ is a continuous Hölder function of order α at x, that is

$$V(x) - V(x+r) \sim r^\alpha \quad \text{for} \quad r \to 0, \tag{2.3}$$

then the following relation applies for the wavelet coefficients:

$$w(r,x) \sim r^\alpha. \tag{2.4}$$

This means that, if $V(x)$ corresponds to a velocity signal, the wavelet coefficient scales as the velocity difference (see also Biferale 1992).

Instead of a continuous wavelet transform, the function $V(x)$ can be decomposed into a series of self-similar orthonormal functions obtained by dilatations and translations of a so-called mother function Ψ_{00} (Meneveau, 1991*a*). By choosing separations $r_k = 2^{-k}$, the set of functions forming the orthonormal basis may be written as

$$\Psi_{kj}(x) = 2^{-k/2}\Psi_{00}(2^k x - j). \tag{2.5}$$

If we consider the signal $V(j)$ sampled on a discrete mesh x_j, the transformed function may be rewritten in discrete form as

$$V(j) = \sum_{r=1}^{\infty}\sum_{i=-\infty}^{\infty} w^{(r)}(i)\Psi^{(r)}(i - 2^r j), \tag{2.6}$$

where now r represents the discretized scale. The wavelet function $\Psi^{(r)}(i - 2^r j)$ is the discretized version of $\Psi^{(r)}(x) = 2^{-r/2}\Psi(\frac{x}{2^r})$ (see Meneveau 1991*a*, for more details) and must obey the following orthogonality condition:

$$\sum_{k=-\infty}^{\infty} \Psi^{(r)}(k - 2^r i)\Psi^{(p)}(k - 2^p j) = \delta_{ij}\delta_{rp}. \tag{2.7}$$

The coefficients $w^{(r)}(i)$ are obtained as

$$w^{(r)}(i) = \sum_{j=-\infty}^{\infty} \Psi^{r}(i - 2^r j)V(j). \tag{2.8}$$

In this paper's data analysis the convolution in (2.8) is performed by means of a fast-wavelet-transform algorithm. In particular, we use Battle–Lemarie wavelet transforms (Mallat 1989, and also Meneveau 1991*a*) which are performed over segments of 4096 samples, that is for a range of 12 degrees of resolution (which we call *scales*). Specifically, the averaging over x (or i), used in the equations which follow, is obtained by computing the wavelet transforms over segments of fixed length, using periodic boundary conditions and a proper windowing technique, and then averaging over them (following the procedure given in Meneveau 1991*b*). Furthermore we checked that the results that are presented in § 6 do not depend upon the choice of the wavelet type.

The principal indicators that we have used for a qualitative analysis of intermittency of the present data, are the following.

Flatness factor (Meneveau 1991*a*), defined as

$$FF(r) = \frac{\langle [w^{(r)}(i)]^4 \rangle_i}{\langle [w^{(r)}(i)]^2 \rangle_i^2}. \tag{2.9}$$

This function (hereafter denoted FF) gives the level of intermittency at the scale r. Therefore, the difference with respect to the Gaussian statistics with flatness factor equal to 3 can be directly evaluated. The subscript i in (2.9) indicates that the average $\langle . \rangle$ is performed over the positions i.

Local intermittency measure (LIM) (Farge 1992), defined as

$$LIM\,(r, i) = \frac{[w^{(r)}(i)]^2}{\langle [w^{(r)}(i)]^2 \rangle_i}. \tag{2.10}$$

This function enhances non-uniform distributions of energy in space since the quantity $[w^{(r)}(i)]^2$ may be interpreted as the energy contained in the signal at the scale r at the

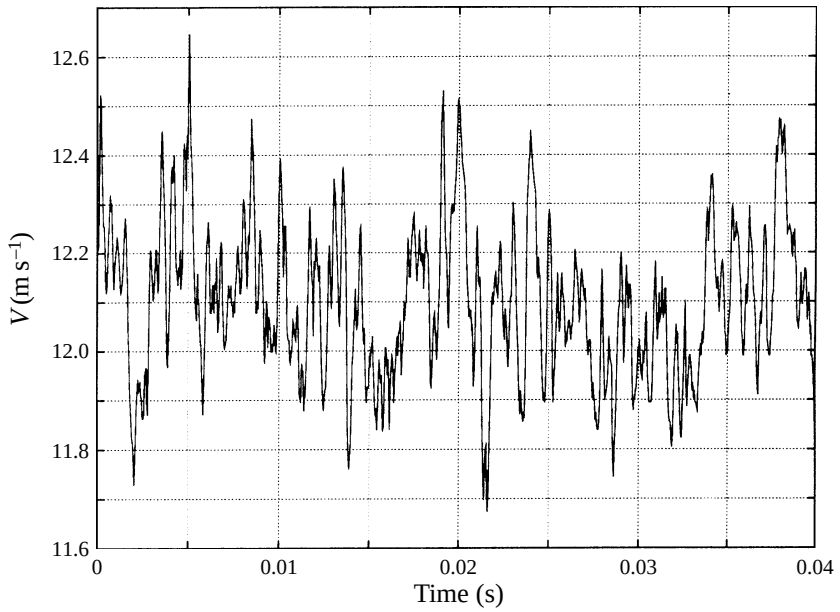

FIGURE 1. Example of a turbulent signal in grid-generated turbulence acquired with a single-probe hot-wire anemometer.

instant *i*. Therefore, the graphical representation of *LIM* at each scale *r* is a good qualitative indicator of intermittency and of the magnitude of the energy fluctuations. Furthermore, as is shown in the next section, peaks in the *LIM* distribution may be associated with the passage of energetic structures which are supposed to be characterized by a high degree of coherence in space.

3. Singularity identification and averaging

An original methodology for educing the energy bursts localized in time and scale is presented in this section. Using this technique, coherent structures are identified and a conditional averaging process is applied so that the shape and energy of the selected structures are quantitatively evaluated. The efficiency, reliability and validation of the method proposed in the following are determined by analysing a numerical signal generated *ad hoc*. The procedure has then been applied to experimental velocity signals and the results obtained are presented in § 6.

An example of a turbulent velocity signal acquired in grid turbulence by means of a single-probe hot-wire anemometer, is shown in figure 1. No structure can be readily identified, and, consequently, there is no apparent connection between the measured intermittency and the passage of turbulent coherent structures. The variation of the velocity magnitude induced by such structures is therefore of the same order or smaller than the velocity fluctuations. Following for instance Kevlahan & Vassilicos (1994), we sometimes refer to vortical structures as flow *singularities*, even if, when dealing with real turbulence, this term cannot be considered in a strictly mathematical sense.

As pointed out by Vassilicos (1996), the wavelet coefficients have the property of enhancing flow singularities, in particular when dealing with Hölder functions as in (2.3). This property may be used to detect singularities in turbulent flows. The

procedure we follow is very simple: first of all, the smallest scale, $\bar{r}$, that can be resolved by the wavelet decomposition must be chosen. This may be done by referring to the usual Fourier spectrum and selecting the smallest wavenumber $k = 2\pi/\bar{r}$ resolved by the probe and not affected by noise. Once $r = \bar{r}$ is chosen, LIM as a function of space x can be computed and a proper trigger threshold level t can be fixed. When, for $x = x_0$, $|LIM(x_0, \bar{r})| > t$, it may be assumed that a particular type of flow singularity has been detected at the position x_0 at the scale $\bar{r}$. By varying the trigger level, one can select singularities of different levels of energy, whereas for $r > \bar{r}$ one can observe singularities corresponding to smaller resolution (or larger scales). The properties demonstrated through the triggering procedure are the following:

Number of singularities: it is of interest to analyse the number of singularities as a function of the trigger level. The number of singularities divided by the total number of samples considered indicates the probability of detecting a flow singularity and this ratio may be interpreted as an indicator of the *space fillingness* of the turbulent structures. We shall compare this function with the expected PDF shapes of the velocity difference fields.

Phase average of the velocity signal: the time signature of flow singularities can be obtained by the ensemble averaging of the velocity signal centred at the position x_0 that corresponds to the sample i_0 where energy overcomes the trigger threshold. If $j = i_0^{(t)}$ is the position where a singularity is detected for a certain trigger level t, we can define $V(j, i)$ as the portion of the velocity signal centred in j and extending for an interval of points i of proper width. The ensemble averaging procedure is then taken over all j where the energy is above the trigger level, and may be written as:

$$V^{(t)}(i) = \langle V(j, i) \rangle_j, \tag{3.1}$$

where, as pointed out above, i extends over an appropriate interval to be chosen in correspondence with the width of the singularity. In continuous form the averaging procedure may be written as

$$V^{(t)}(x) = \langle V(x - x_0) | \{x_0\} \rangle_{x_0},$$

which indicates that the procedure leads to a statistical averaging conditioned on the events x_0. By varying the resolution where the peaks' detection is performed, it is possible to observe structures of different size. This procedure is similar to the averaging process proposed by Kevlahan & Vassilicos (1994) for *local* and *global* similarity to be distinguished. The advantage of the present procedure is that the time signature of a coherent structure passing through the measurement volume can be directly observed on the velocity signal whereas in the case of Kevlahan & Vassilicos (1994), the averaging is performed on the wavelet coefficients so that structure shape in the time domain is not differentiated. They obtain superimposed *cones* in the wavelet domain, indicating the presence of singularities. Furthermore, their procedure is particularly efficient at high Re (or for velocity signals with a very large range of length scales).

To test the procedure proposed in the present work, the averaging process is applied to an artificial Gaussian random velocity signal superimposed on singularities given by (2.3) with exponent $\alpha = -1/6$. The total number of points is 10^6. Specifically, the Gaussian signal has zero mean value and a standard deviation of about 0.5. The singularity distribution is instead characterized by a much smaller standard deviation (of about 0.004), two orders of magnitude smaller than that of the Gaussian signal. As is shown later, the adopted ratio between singularities and global signal standard deviations is of the same order as what is observed in real turbulence. Therefore it is

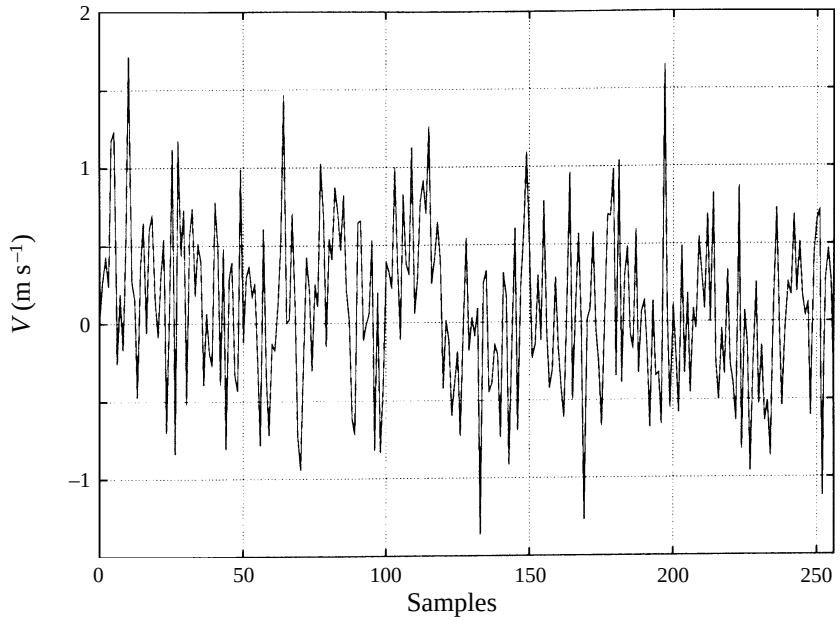

FIGURE 2. Singularities superimposed on a Gaussian random signal (see (2.3)). The presence of singularities cannot be identified.

impossible to identify singularities on the resulting signal without a proper averaging technique. This is demonstrated by figure 2 where one segment of the resulting signal is reported. In figure 3 the averaged signal is presented. The random oscillations are almost eliminated whereas the contribution of singularities is enhanced. A further check has been performed by comparing the energy contained in the reconstructed singularities to the energy associated with the real ones. Specifically, supposing that the artificial signal corresponds to velocity *vs.* time x, the energy for unit time contained in the total number of singularities may be defined as

$$E = \frac{\int V(x)^2 \mathrm{d}t \times N_s}{X_{tot}}, \tag{3.2}$$

where the integral extends over the time interval corresponding to the length of the singularity. N_s is the number of singularities whereas X_{tot} is the total acquisition time window (corresponding, in the present case, to 10^6 samples). The energy E has been calculated for the singularities given by (2.3) (indicated as E_r), and for the singularities identified by the averaging process (hereafter indicated as E_a). It has been found that the agreement is quite satisfactory since the relative error, defined as $(E_r - E_a)/E_r$, is about 5%, since $E_r \simeq 0.020$ and $E_a \simeq 0.019$. It has to be pointed out that a possible source of error in the averaging technique is related to the loss of resolution yielded by the wavelet decomposition. When N samples are transformed, the largest available resolution corresponds to $N/2$ samples. This leads, on the reconstructed time signal, to a phase uncertainty corresponding to 1 sampling interval. When dealing with strongly peaked functions, as in the case of (2.3), this may lead to a slight error in the peak magnitude reconstruction and, consequently, in the energy estimation. Nevertheless, in the case of real turbulence data the shape of the averaged singularities is smoother

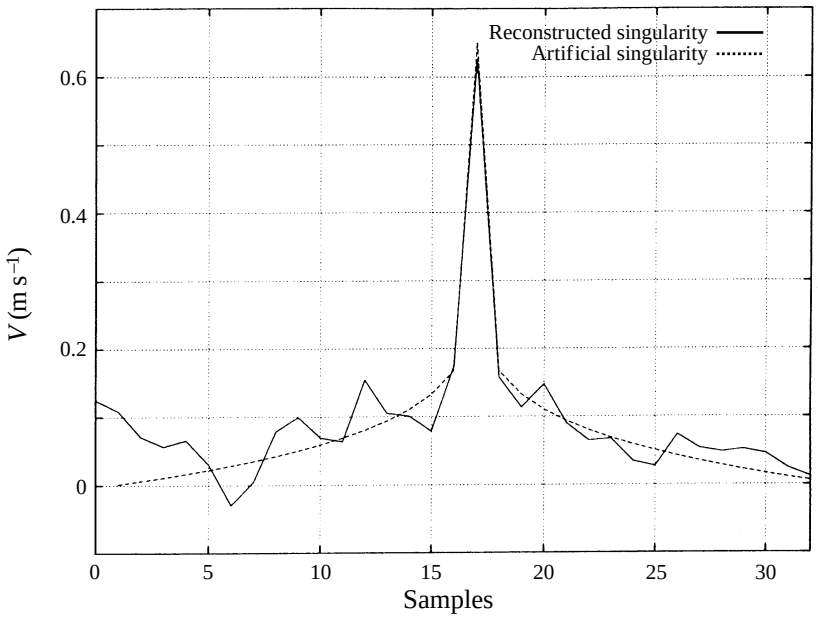

FIGURE 3. The result of the averaging procedure applied to the signal of figure 2. The singularities are now clearly enhanced and their shape is correctly reconstructed (the functional form of singularities is $[x - x_0]^{-1/6}$).

because of the effect of viscosity. Therefore the error is very low and this source of uncertainty has not been accounted for.

4. Extended self-similarity

The calculation of the intermittency exponents of (1.1), at low and moderate Re_λ, can be accurately performed by the use of the ESS form of scaling, recently introduced by Benzi *et al.* (1993*a*) and Benzi, Ciliberto & Chavarría (1995) (see also Arneodo *et al.* 1996 and Benzi *et al.* 1996 for extensive discussion of the properties of ESS). This form of scaling permits the detection of a widely extended scaling range, even for low and moderate Re_λ and for scales inside the dissipation range. Owing to this interesting property, several studies have been performed in this field (see also Briscolini & Santangelo 1994; Camussi & Guj 1996; Camussi *et al.* 1996*a*). The range of scales where a scaling law applies is found by determining the scaling of the absolute value of one structure function with respect to the absolute value of the third-order one, i.e.

$$\langle |\Delta V(r)|^p \rangle \sim \langle |\Delta V(r)|^3 \rangle^{\zeta(p)}, \tag{4.1}$$

where the use of the absolute value improves the statistical convergence (Camussi *et al.* 1996*b*). It has been found that the ESS scaling range applies all the way down to scales of the order of a few Kolmogorov lengths (about $r \sim 5\eta$), which is deep inside the dissipation range of scales. Furthermore the scaling exponents calculated from (4.1) are almost independent of Re_λ (Arneodo *et al.* 1996). One question that we would like to clarify in this paper is whether this form of scaling still applies for the wavelet coefficients at low Re_λ. Indeed, as shown in § 2, the wavelet coefficients scale as the velocity differences (2.4). Therefore it is possible to verify if the following

$\overline{V}$ (m s^{-1})	σ_V (m s^{-1})	η (mm)	λ (mm)	Re_λ	$N_{tot} \times 10^5$	$F_s \times 10^3$ (s^{-1})
1.4 (I)	0.0066	~2.80	~9.2	~ 3	30	16
2.5 (I)	0.0290	~0.80	~6.3	~ 12	30	16
5.1 (II)	0.0521	~0.50	~3.7	~ 20	5	35
11 (III)	2.3500	~0.05	~1.7	~ 250	42	24
8.4 (IV)	2.0310	~0.10	~7.0	~ 800	160	16

TABLE 1. Characteristic parameters of the different flow conditions: (I) represents homogeneous grid turbulence ($x/M = 163$, with M the grid mesh size) at very low Re_λ, (II) represents the experiment in homogeneous grid turbulence at $Re_\lambda \simeq 20$, (III) is fully developed jet turbulence at $x/D_1 = 23$ (where D_1 is the jet diameter) and (IV) also jet turbulence at $x/D_2 = 25$ ($D_2 = 3\ D_1$). $\overline{V}$ is the mean axial velocity at the measurement positions and σ_V is the longitudinal standard deviation. N_{tot} is the total amount of acquired samples with frequency sampling indicated as F_s. Also, η is the Kolmogorov length, defined as $\eta = \nu^{3/4}\epsilon^{-1/4}$, whereas λ is the Taylor microscale.

relation applies for the low Re_λ considered in the present work:

$$\langle |w^{(r)}(i)|^p \rangle_i \sim \langle |w^{(r)}(i)|^3 \rangle_i^{\zeta(p)}. \tag{4.2}$$

Furthermore, it is possible to apply this equation only to the flow singularities selected by the triggering procedure previously explained. For a certain trigger level t, it is then possible to write the following relation:

$$\langle |w^{(r)}(i^{(t)})|^p \rangle_{i^{(t)}} \sim \langle |w^{(r)}(i^{(t)})|^3 \rangle_{i^{(t)}}^{\zeta(p)}. \tag{4.3}$$

The use of (4.3) corresponds to checking the validity of ESS in connection with the presence of a flow singularity. The consequences of such a procedure are discussed in § 6.

5. Flow conditions

The experimental analyses have been conducted in different turbulent flow conditions by means of constant-temperature anemometers (CTA) with single sensor and X probes. The statistical reliability and experimental uncertainty of all the data considered has been thoroughly verified in previous works (Camussi & Guj 1996 and Camussi *et al.* 1996*a–c*). In particular, homogeneous grid-generated turbulence has been considered at low and very low Re_λ (down to $Re_\lambda \simeq 3$) whereas fully developed jet turbulence has been studied at moderate and high Re_λ (up to $Re_\lambda \simeq 800$). The principal flow conditions and acquisition parameters are summarized in table 1. Details on experimental arrangements, data processing and accuracy evaluation can be also found in Camussi & Guj (1996) and Camussi *et al.* (1996*a–c*).

6. Results and discussion

The use of wavelet decomposition has allowed us to correlate two important aspects of turbulence in the transition from fully developed ($Re_\lambda \simeq 800$) to almost laminar conditions ($Re_\lambda \simeq 3$): small-scale intermittency and the presence and shape of small-scale coherent structures.

The first point, widely studied in recent years, refers to small-scale intermittency. In the present work attention is focused on the analysis of intermittency at low Re_λ. The present application of the wavelet transform in connection with the use of a

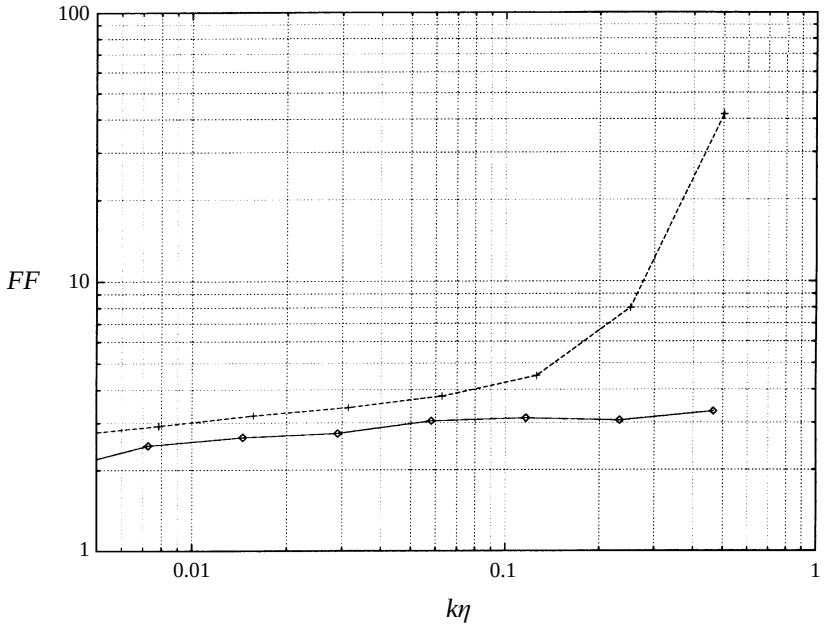

FIGURE 4. *FF* calculated for homogeneous turbulence at $Re_\lambda \simeq 3$ (solid line) and $Re_\lambda \simeq 12$ (dashed line). At large scales (small resolution) the statistics is close to Gaussian and *FF* is close to 3.

trigger threshold in the structure identification procedure permits *universal* properties of the scaling relations which are observed for $Re_\lambda \geqslant 10$ to be found. The intermittent behaviour is also analysed through other qualitative indicators and by the evaluation of wavelet coefficient scaling exponents.

The second aspect, still under debate, is the presence and the shape of small-scale coherent structures, which in the present cases are identified by a suitable conditional averaging technique. It is shown that coherent structures, in the experiments considered, have shapes which may depend upon the *turbulence generator*.

6.1. *Intermittency at low* Re_λ

Qualitative indicators of intermittency are *FF* and *LIM* defined in § 2. One result in terms of *FF* at $Re_\lambda \simeq 12$ and $Re_\lambda \simeq 3$ and in homogeneous conditions, is reported in figure 4. *FF* is plotted as a function of the non-dimensional wavenumber $k = 2\pi/r$, where r denotes the scale and the normalizing factor adopted is the Kolmogorov length η (see Meneveau 1991*a*). An increase in magnitude of *FF* at $Re_\lambda \simeq 12$ is observed at the smallest scales (i.e. for large resolution) indicating the departure from a Gaussian distribution (corresponding to $FF = 3$) as an effect of intermittency (according to Meneveau 1991*a*, figure 8) whereas *FF* calculated at $Re_\lambda \simeq 3$ remains approximately constant and close to 3, indicating the absence of intermittency at any scale. The deviations from the Gaussian distribution are expected for high Re_λ but the result of figure 4 shows that even for $Re_\lambda \simeq 12$ intermittency effects at small scales are significant (see e.g. She, Jackson & Orszag 1988, and Camussi & Guj 1996).

The value of *LIM* at different scales gives further qualitative information on the degree of intermittency which characterizes different flow conditions. In particular, we focus attention on the smallest scales resolved which, as already pointed out, can be selected by the Fourier spectra analysis. In figure 5 *LIM* calculated in homogeneous grid turbulence, at two different Re_λ, are reported. The intermittent nature of the

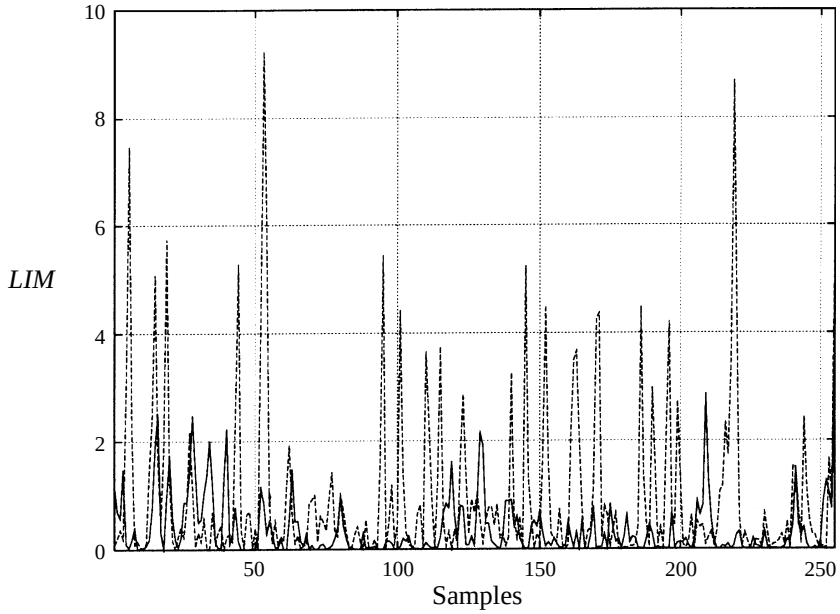

FIGURE 5. *LIM* calculated at the smallest resolved scale for homogeneous grid turbulence at $Re_\lambda \simeq 3$ (solid line) and 12 (dashed line). The highest peaks indicate the presence of coherent structures which are supposed to correspond to a high energy level. Note that the integral of *LIM* reported in the figure may be slightly different from the expected unity value since the plot corresponds to a segment of 256 samples from a series of 4096 samples.

energy distribution is well demonstrated by the non-uniform distribution of the peaks. By definition, the peaks of *LIM* are related to energy *bursts* at the selected scale r, therefore $LIM = o(1)$ indicates no intermittency, whereas the largest peaks are presumed to be induced by the passage of structures of high spatial coherence in the turbulent flow. More specifically, figure 5 shows that at $Re_\lambda \simeq 3$ the *LIM* distribution is characterized by small fluctuations, whereas the degree of intermittency is significantly higher at $Re_\lambda \simeq 12$.

This preliminary analysis indicates, from a qualitative point of view, that intermittency is observed at least for $Re_\lambda \geqslant 10$. This is confirmed by the *FF* and *LIM* analyses conducted in other flow configurations at higher Re_λ which, for brevity, are not reported here. Indeed, the *FF* and *LIM* have similar behaviours for $Re_\lambda \geqslant 10$, whereas for $Re_\lambda < 10$, no significant increase in the *FF* magnitude and no significantly peaked distributions of *LIM* are observed.

As indicated in (4.2), it is possible to verify the validity of ESS when applied to the wavelet coefficients. This analysis has been previously conducted by Arneodo *et al.* (1996), but we extend this study to lower Re_λ. An example of the scaling ranges detected by the ESS in homogeneous grid turbulence ($Re_\lambda \simeq 12$) and for p ranging from 2 to 6, is given in figure 6. A scaling range is observed and the scaling exponents, calculated by linear fits also represented in the figure, are, as indicated in table 2, in agreement with previous results at higher Re_λ, and also with exponents obtained by the ESS applied to the same data, but using the velocity structure functions (Camussi & Guj 1996). The exponent uncertainty has been evaluated by the standard deviations of the PDFs of all the possible slopes that can be obtained by couples of points in the scaling range (Camussi *et al.* 1996*a*). The linear fits are conducted over an interval

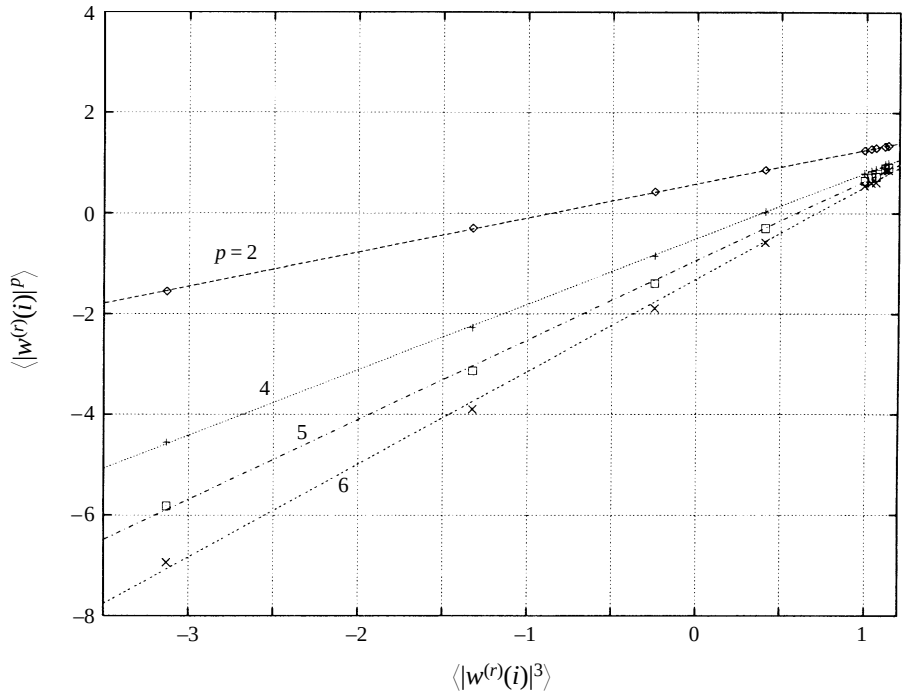

FIGURE 6. Scaling ranges obtained by means of the ESS form of scaling for $p = 2,\ 4,\ 5,\ 6$ in homogeneous grid turbulence at $Re_\lambda = 12$. The linear fits correspond to the straight lines and the scaling exponents are reported in table 2.

p	K41	B. *et al.*	ESS*	Present results
2	$0.6\overline{6}$	0.70	0.68	0.68 ± 0.002
4	$1.3\overline{3}$	1.28	1.30	1.30 ± 0.012
5	$1.6\overline{6}$	1.53	1.54	1.56 ± 0.021
6	$1.9\overline{9}$	1.78	1.83	1.84 ± 0.022

TABLE 2. Comparison of the measured exponents to the Kolmogorov theory (indicated as K41) and the experimental results of Benzi *et al.* (1993*a*) (indicated as B. *et al.*). ESS* represents the scaling exponents obtained from ESS applied to the same data but using the velocity structure functions (4.1).

corresponding to scales larger than the dissipative length η and smaller than the integral one. Also the analysis of other cases considered (not reported here) confirms that the scaling exponent magnitudes are in agreement with previous results, e.g. those of Benzi *et al.* (1993*a*), and that down to $Re_\lambda \simeq 10$, through ESS, it is possible to demonstrate an intermittent behaviour characterized by the same scaling exponents as the high-Re_λ cases.

Further properties may be obtained following the triggering procedure explained in § 3. By varying the trigger level, a different number of singularities is detected. Since intermittency is related to coherent structures, which in the present case are interpreted as energy *bursts* corresponding to singularities in the *LIM* distribution, ESS should also apply when considering only those *events* if they are responsible for intermittency. In figure 7 the pth ($p = 2,\ 4,\ 5,\ 6$) vs. third-order moments are shown

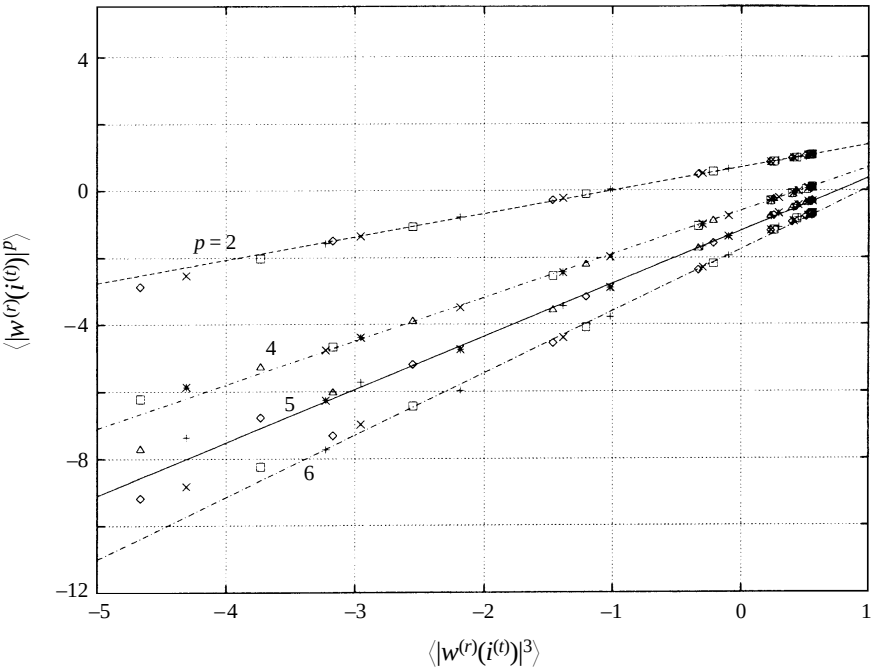

FIGURE 7. Scaling ranges obtained by means of ESS for different trigger levels and for $p = 2, 4, 5, 6$. Four trigger levels t_i (with $i = 1...4$) are considered at each p (corresponding, for a certain p, to different symbols) such that $t_i/t_{i+1} = 2$. The collapse of the points is satisfactory indicating the independence of the scaling exponents with respect to the trigger threshold. The figure corresponds to homogeneous grid turbulence at $Re_\lambda = 12$.

for the case of homogeneous grid turbulence at $Re_\lambda = 12$ and for different trigger levels. The collapse of the points is satisfactory in all cases and the linear fit gives the expected exponent with an error down to 1% with respect to the $\zeta(p)$ calculated by (4.2) (see the fifth column of table 2). Similar results (not reported here) are obtained for the other flow conditions at larger Re_λ whereas at $Re_\lambda = 3$ the expected *regularization* of the scaling exponents is observed (Camussi & Guj 1996). Specifically, for very low Re_λ or for scales $r \leqslant \eta$, the regularization implies that $\langle \Delta V(r)^p \rangle \sim r^p$ (e.g. Monin & Yaglom 1975), therefore a Kolmogorov $p/3$ scaling is observed when the ESS is used, that is when $\langle \Delta V(r)^p \rangle$ is plotted against $\langle \Delta V(r)^3 \rangle$. These results indicate that ESS is a property which characterizes the scaling of singularities when $Re_\lambda \geqslant 10$. The scaling behaviour, indeed, does not vary when only singularities responsible for intermittency are conserved. This supports the robustness of ESS as a correct way for observing scaling laws and confirms that only singularities are responsible for the observed intermittent behaviour.

From a practical point of view, the determination of the scaling exponents by the triggering procedure may be performed by considering not the *background* turbulence but only the time instants corresponding to the selected *events*. This may lead to a significant decrease of the number of samples that it is necessary to process in order to obtain the scaling exponents. As an example, in the present case, the use of the triggering method in addition to the ESS leads to the correct scalings, by using a total amount of data of about two orders of magnitude smaller than the acquired ones. The triggering procedure may then be inserted in the measurement chain, allowing

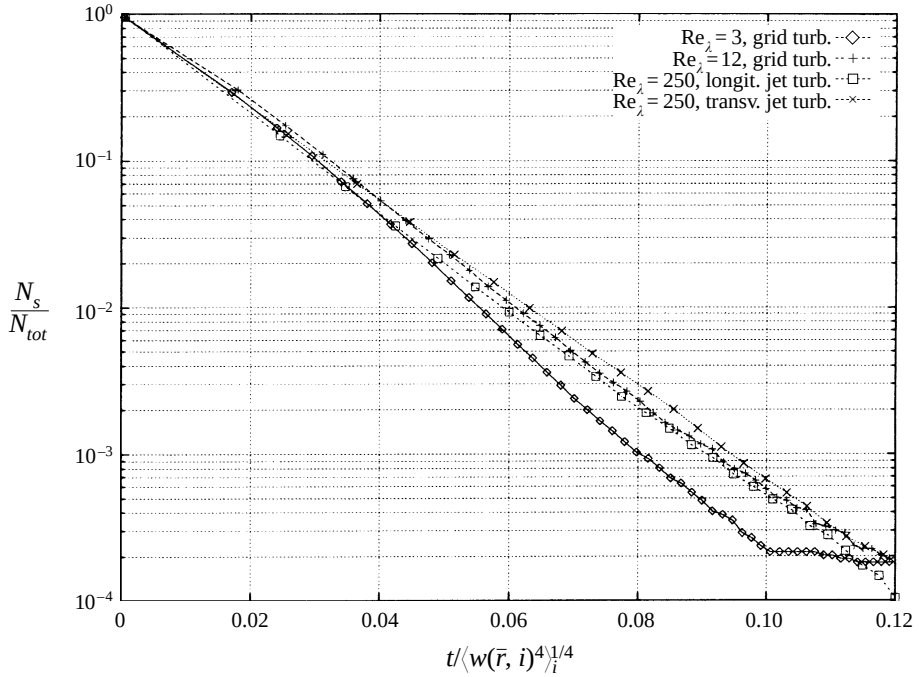

FIGURE 8. Number of singularities as a function of the trigger threshold level properly normalized. The curves represent different flow conditions in homogeneous turbulence. The collapse of the curves, except for the lowest Re_λ ($\simeq 3$), is achieved in all cases.

a (quasi)real-time selection of the samples of interest. The implementation of this procedure is presently under study by the authors.

As already pointed out, the number of singularities normalized with respect to the total number of samples, indicates the *space fillingness* of singularities at different energy levels. Furthermore, since $\langle w(r,i)\rangle_i \sim \Delta V(r)$, the ratio between the number of singularities and the total amount of samples is directly related to the PDFs of the velocity differences. Accounting for the proportionality between *LIM* and the square of the wavelet coefficients, i.e. the energy contained at the selected scale, we introduce a new normalization in order for intermittency to be accounted for in each flow condition. An example concerning homogeneous grid turbulence and jet turbulence is presented in figure 8. Here, the curves are normalized with respect to the r.m.s. of *LIM* calculated on the selected scale where the trigger threshold acts. Such a scale is chosen as the smallest resolved scale and then actually varies for the different flow conditions. Indicating by t the threshold level and $\bar{r}$ the selected scale, the following non-dimensional expression is obtained:

$$\frac{N_s}{N_{tot}} = f\left(\left[\frac{t}{\langle LIM\,(\bar{r}, i)^2\rangle_i^{1/2}}\right]^{1/2}\right), \tag{6.1}$$

where N_s is the number of singularities and N_{tot} is the total number of samples which is considered in the averaging procedures. By simple manipulation and accounting for the definition of *LIM*, it may be shown that the previous expression corresponds

to

$$\frac{N_s}{N_{tot}} = f\left(\frac{t^{1/2}}{FF(\bar{r})^{1/4}}\right), \tag{6.2}$$

or to the following explicit relation:

$$\frac{N_s}{N_{tot}} = f\left(\frac{t}{\langle w(\bar{r}, i)^4\rangle_i^{1/4}}\right). \tag{6.3}$$

The quantity $\langle w(r, x)^4\rangle_i^{1/4}$ is therefore dependent on both the degree of intermittency and the energy contained at the scale $\bar{r}$. Equation (6.2) represents the new normalization adopted as applied in figure 8. In this figure, except for the case at $Re_\lambda \simeq 3$, the collapse of the curves is satisfactory showing a universal feature of such distributions for $Re_\lambda \geqslant 10$. Also, the functional form is in agreement with previous observations (Gagne 1987). It should be pointed out that the collapse of the curves is achieved only when the exponent p of the normalizing factor $\langle w(r, x)^p\rangle_i^{1/p}$ equals 4. This may be related to the direct connection between flatness and degree of intermittency. It should be pointed out, indeed, that the normalizing factor is related to the *LIM* r.m.s., which gives an indication of the mean fluctuations of energy and, therefore, gives an estimate of the degree of intermittency. Finally, the use of a semi-log scale in figure 8 demonstrates the exponential functional form of the curves in agreement with previous results on the velocity difference PDFs (e.g. Castaing *et al.* 1990).

As a conclusion, the results obtained so far confirm that, even in those cases where intermittency is hardly detected (i.e. for $Re_\lambda \simeq 10$), singularities are still present. Furthermore, the dimensionless number of singularities presents the same exponential law as the cases at higher Re_λ. Therefore the presence of intermittency and the mechanism of formation of singularities of different energy, may be extended from high to very low turbulence, that is for $Re_\lambda \geqslant 10$.

6.2. *Averaged velocity induced by coherent structures*

The triggering procedure presented in § 3, has been used to detect the averaged time signatures corresponding to the peaks selected in the *LIM* distributions. We point out that the variation of the resolution r where *LIM* is calculated corresponds to analysing the effect of intermittency detected at different scales. In principle, it is not possible to affirm that intermittency at small (large) scales is induced by small (large) structures. This aspect is demonstrated below in the framework of the jet signals analysis.

The average of coherent-structure signatures obtained in homogeneous and isotropic grid turbulence at $Re_\lambda \sim 12$ is presented for different trigger levels in figure 9. Specifically, indicating with t_1, t_2 and t_3 the three different thresholds, we have $t_1 < t_2 < t_3$ with $t_1/t_2 = 0.2$ and $t_1/t_3 = 0.1$. The x-axis represents the space scale normalized with respect to the Kolmogorov length η. The relative velocity of the y-axis, is instead normalized with respect to the r.m.s. velocity fluctuations. The latter quantity is strictly related to the total amount of energy of the signal. Therefore, the normalized velocity may be interpreted as the relative energy associated with the intermittent structures with respect to the energy contained in the velocity fluctuations of the whole signal. This normalization has been adopted in all the figures that follow. Note that the average extracted structures have higher intensity for higher trigger levels because lower trigger levels include information from lower energetic structures in addition to that captured by using higher trigger levels. From figure 9, it is evident

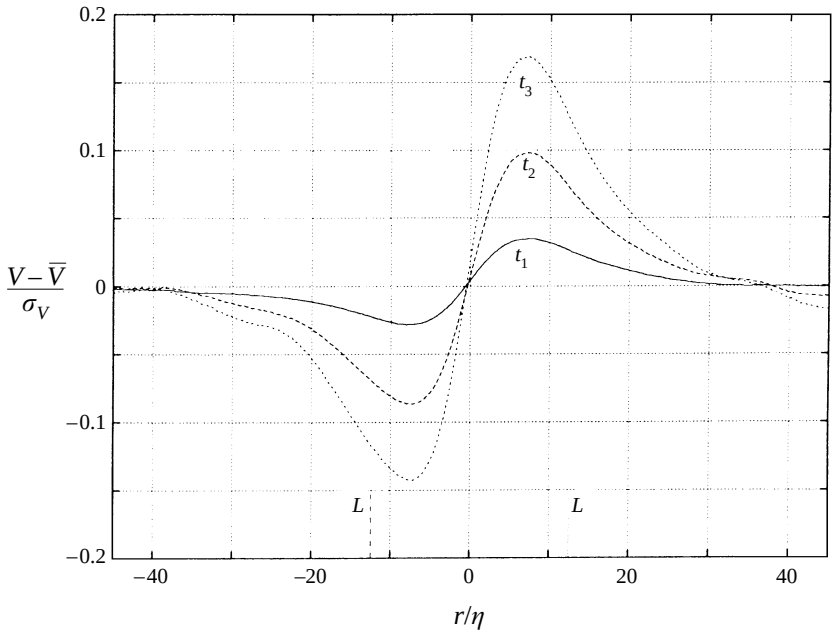

FIGURE 9. Turbulent structure signatures on the velocity signal in homogeneous turbulence at $Re_\lambda = 12$. Different curves corresponds to different trigger threshold levels with $t_1 < t_2 < t_3$. L represents the integral length in terms of η.

that the passage of coherent structures has been identified, for any trigger level. The averaged signal is reminiscent of the velocity profile in a Rankine vortex tube. The geometric scale of the structures detected does not depend upon the trigger level, thereby demonstrating the robustness of the identification technique adopted. Also, in all the other cases considered, the extent of the structures identified, in terms of r/η, does not depend upon the trigger level. Therefore, in the figures which follow, only one value of t is considered.

By selecting the resolution (that is by varying the scale r where the *LIM* thresholding is applied) it is possible to detect structures of different size. In the cases of grid turbulence, shown in figure 10(a, b) respectively for $Re_\lambda \sim 12$ and 20, it is observed that the larger the resolution the smaller the structures identified. This behaviour is clearly observed even if in these cases the L/η ratio (L represents the integral length) is small. The characteristic size of the structures corresponding to the smallest resolved scales is qualitatively evaluated from the peak-to-peak distance. Such scales are of about 8η–10η for both Re_λ. The larger structures, obtained with a resolution 2^4 times smaller, have instead the size of about one integral length. Furthermore, we have calculated the ratio between the energy contained in small- or large-scale structures eductedby fixing the trigger level $t_i = 2$, and the total energy of the signal (see (3.2)), that is E_a/σ_V^2. In this way, we may estimate the contribution of the educted coherent structures to the total energy of the signal. In the case of small-scale structures, the energy ratio is about 1% of the total energy whereas, for the largest scales, it is on the order of 10%. The sensitivity of the estimated energy E_a to t_i has been checked to be weak.

The case at $Re_\lambda = 3$ is reported in figure 11. For such low Re_λ, the turbulent structures have, for different resolutions, a scale which remains always approximately

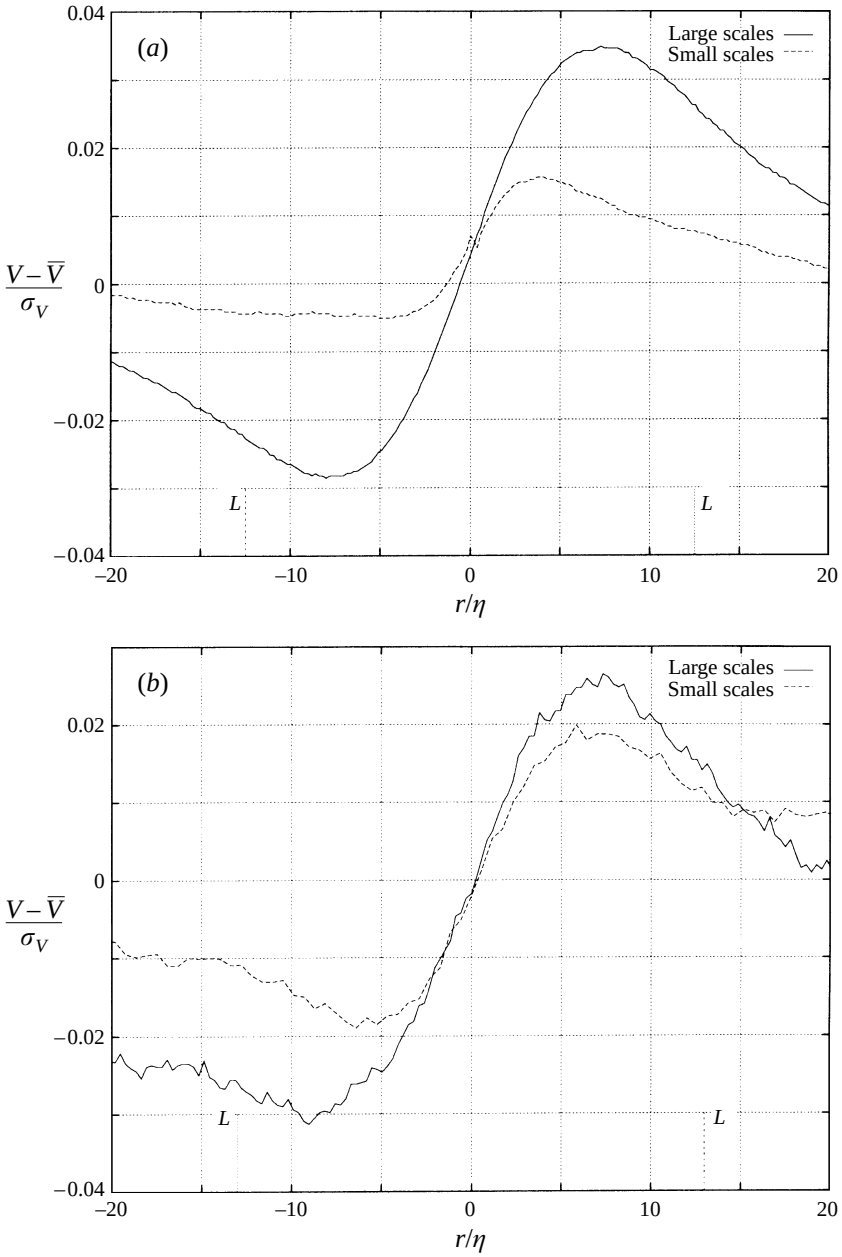

FIGURE 10. Turbulent structures corresponding to different resolution, obtained for homogeneous grid-turbulence at $Re_\lambda = 12$ (*a*) and $Re_\lambda = 20$ (*b*). The large-scale signal of (*a*), corresponds to the lower curve (lower trigger level) of figure 9. The greater smoothness of the curves of (*a*) with respect to (*b*) is related to the larger number of samples acquired. The size of the structures is on the order of 8η for (*a*) and about 10η for (*b*). The integral lengths are also shown.

on the order of the integral length. The large magnitude of the characteristic size of the turbulent structure and the small integral-to-Kolmogorov length ratio may be the cause of the low degree of intermittency observed at such low turbulence levels. On the other hand, because of the low intermittency, it was expected that coherent structures

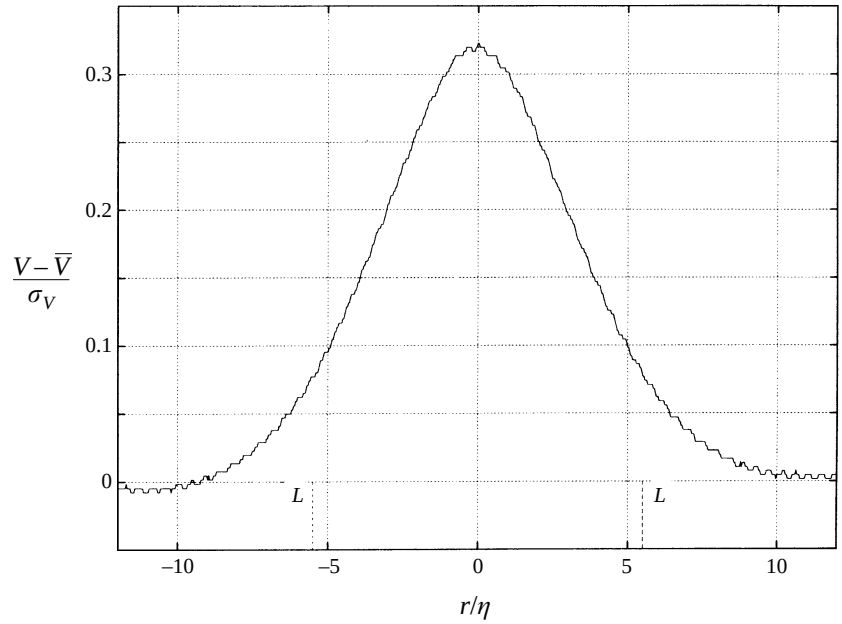

FIGURE 11. Turbulent structure detected for $Re_\lambda = 3$. In this case the change of resolution does not lead to smaller structures. The integral length is shown.

were characterized by a large size. In fact, the normalized velocity amplitude (that is correlated to the relative energy of the turbulent structure) is larger than in previous cases where intermittency was present and the energy ratio E_a/σ_V^2 is of the order of 10%.

On the other hand, quite different averaged velocity signatures are identified in the case of the turbulent jet. The longitudinal and transverse components of the velocity signatures are presented in figure 12(*a*). Also in this case, the variation of resolution does not lead to any change in the structure size, for both velocity components. In fact, from a qualitative point of view, the averaged velocity signals seem, in these cases, to be induced by the passage of a vortex ring around the probe, i.e. a large-scale structure with high relative energy level. When a vortex ring, generated in the mixing layer region of the jet flow, approaches the probe position the longitudinal velocity magnitude measured increases, then has a maximum when the ring passes through the measuring position, and finally decreases. The transverse velocity induced by such large-scale structures is on the other hand always zero for symmetry. Therefore, zooming in on the transverse velocity component of figure 12(*a*), we may observe time signatures of turbulent coherent structures passing through the axis of the jet flow, since the transverse velocity is not affected by the passage of rings. The result is reported in figure 12(*b*). The coherent-structure time signature appears very similar to those observed in homogeneous grid turbulence at $Re_\lambda \geqslant 10$ (figures 9 and 10). The relative velocity amplitude is of the same order as, but slightly lower than that of figure 10(*a*, *b*). In the case of figure 12(*b*), the filtering effect due to the X probe length, which corresponds to about 20η, may affect the resolution of the averaging process so that the amplitude of the smaller structures, as well as their contribution to the averaged velocity, may be reduced. In terms of energy, we observed that small-scale structures (always educted for $t_i = 2$), obtained from the transverse components, gives a ratio E_a/σ_V^2 of the order of 1% whereas the large structures observed on

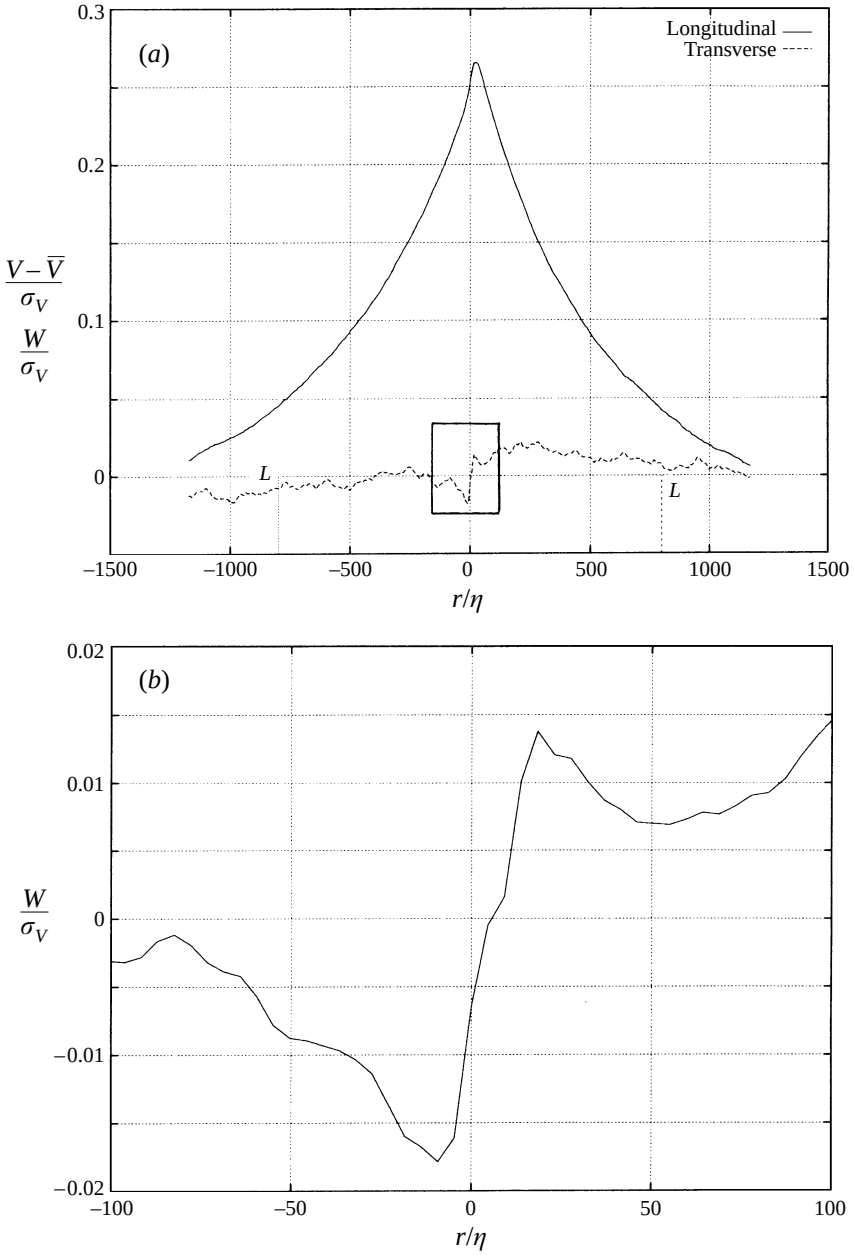

FIGURE 12. (*a*) Longitudinal and transverse velocity signature of turbulent structures in jet turbulence at $Re_\lambda = 250$. (*b*) A blow up of the highlighted region of (*a*) corresponding to the transverse velocity component. W and σ_W represent respectively the transverse and r.m.s. velocity. Integral length is shown in (*a*).

the longitudinal component appears much more energetic since the E_a/σ_V^2 ratio is about 30%. This estimations are based on the structures extracted with $t_i = 2$ but, as pointed out above, are qualitatively valid for any t_i.

In order to validate this result further, we applied the triggering procedure to turbulent signals acquired with a single micro-probe hot-wire anemometer, in a

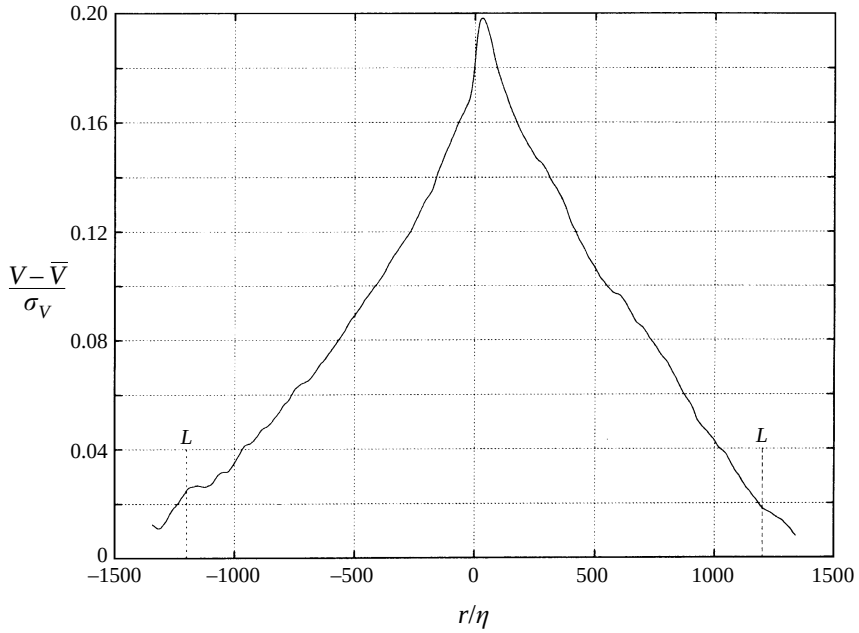

FIGURE 13. Longitudinal velocity signature of turbulent structures in jet turbulence at $Re_\lambda = 800$. The agreement with the previous longitudinal component in jet turbulence (figure 12*a*) is evident. The integral length is also shown.

turbulent flow generated by a jet with large diameter and at high Re_λ ($\simeq 800$, that is case (IV) of table 1). In this case the probe resolution is much better than in the previous jet signals (probe length $\sim 4\eta$), but only the longitudinal velocity component has been measured. The result obtained is shown in figure 13 confirming the shape already observed in the corresponding longitudinal velocity of figure 12. Furthermore, also in this case, we found that the E_a/σ_V^2 ratio is of the order of about 30%.

In summary, in the case of turbulent jets, the longitudinal velocity component permits the identification of the mixing layer structures (vortex rings), whereas the transverse velocity component reveals the presence of intermittent structures, similar to those observed in homogeneous grid turbulence. Furthermore, note that the intermittent small coherent structures (differentiated through the transverse component) are strongly correlated with the structures of larger scale (differentiated through the longitudinal component) since they correspond to the same time instants (indicated with j in (3.1)). The energy associated with these large structures seems to overcome, in some cases by one order of magnitude, that associated with the smaller structures which have been used for phasing the averaging process. Therefore, intermittency at the smallest scales may be induced by structures of much larger size (of the order of the integral length).

7. Conclusions

Several aspects concerning intermittency and coherent structures in low- and moderate-Re_λ homogeneous turbulence have been addressed through the orthogonal wavelet decomposition in combination with the ESS form of scaling, applied

to experimental data obtained in grid and jet turbulent flows. The principal results obtained, are summarized as follows.

The ESS form of scaling applies for the wavelet coefficients and yields intermittency exponents in agreement with previous analyses based on the scaling of the velocity structure functions at the same and much higher Re_λ.

The qualitative indicators *FF* and *LIM* confirm that intermittency and the consequent anomalous scalings are properties not only of the inertial range, but they may be extended to the dissipative region or to very low-Re_λ flows (down to $Re_\lambda \geqslant 10$).

Singularities of the turbulent flows are identified as energy bursts at the smallest scales. It is observed that only such singularities are responsible for intermittency and that ESS still applies when only these events are considered and the turbulent background is eliminated. The anomalous scaling is indeed still observed even when the time selected for the scaling analysis, correlated with the triggered events, is of about two orders of magnitude less than the total time acquisition length. This suggests that the energy contained by the small-scale turbulent structures responsible for intermittency is only a small percentage of the total energy of the turbulent velocity fluctuations and seems in agreement with previous numerical results concerning the contribution of vortex tubes to the total turbulent energy (e.g. Jiménez *et al.* 1993).

Turbulent structures are detected in all cases even for $Re_\lambda \simeq 3$, that is at a very low turbulence level for which intermittency anomalies are totally absent. The presence of coherent structures may then be assumed as a property of homogeneous turbulence independently of Re_λ.

The space fillingness of the identified coherent structures is weakly dependent on Re_λ if homogeneity is preserved. In fact, a new normalization is introduced and, in homogeneous conditions, universal behaviour is observed for $Re_\lambda \geqslant 10$ but not for $Re_\lambda \simeq 3$. Therefore, the lower limit, in terms of Re_λ, to detect intermittency anomalies using the ESS technique coincides with that required in order for a universal behaviour of the space fillingness of coherent structures to be observed.

A conditional averaging technique based on the triggering procedure applied to the *LIM* distributions at different scales or resolutions is presented and validated. This procedure allows us to observe the time signature of the passage of coherent structures close to the measurement position.

In homogeneous grid-generated turbulence, the averaged time history seems to be related to the passage of vortex tubes even though only a three-dimensional analysis would be able to clarify the actual shape of the structures. At the smallest scales, the size of the extracted average structures is on the order of 4η–5η (according to Jiménez *et al.* 1993). At $Re_\lambda = 3$, where no intermittency is observed, structures with broader characteristic scale are observed. The latter seems to be the effect which leads to the disappearance of intermittency.

In jet turbulence, the longitudinal velocity component seems to be affected by the passage of vortex rings belonging to the mixing layer region. Such large structures induce intermittency even on the smallest scales, where the triggering procedure is applied. Furthermore, the large structures are in phase with the smallest ones which instead seem to conserve a filamentary shape. It is confirmed that small-scale structures contribute a small percentage to the total energy whereas the energy of the large-scale structures may reach 30% of the total.

The most significant result obtained from the conditional averaging procedure is that structures with different shape and of very large scale seem to induce intermittency with universal scaling exponents. Indeed, recall that the $\zeta(p)$ exponents corresponding to the longitudinal velocity component, measured in jet or grid turbulence, are always

the same (see e.g. Benzi *et al.* 1993*a*). Therefore, the possible different nature of coherent structures is hidden behind the *universality* of the scaling exponents usually observed both in grid and in jet turbulent flows.

G. Solla is gratefully acknowledged for his support and collaboration in the implementation and development of software for the wavelet analysis. R. Verzicco is acknowledged for his helpful comments and suggestions. C. Meneveau is also acknowledged for having rendered available the CTR report. We thank F. Stella and D. Barbagallo for their contribution to the measures performed at the University of Rome, and S. Ciliberto and C. Baudet for their help during the measures performed at the ENS de Lyon. This research has been supported by MURST 40% (1993).

REFERENCES

Anselmet, F., Gagne, Y., Hopfinger, E. J. & Antonia, R. A. 1984 High-order velocity structure functions in turbulent shear flows. *J. Fluid Mech.* **140**, 63–89.

Arneodo, A., Grasseau, G. & Holshneider, M. 1988 On the wavelet transform of multifractals. *Phys. Rev. Lett.* **61**, 2281–2284.

Arneodo, A., Baudet, C., Belin, F. *et al.* 1996 Structure functions in turbulence, in various flow configurations, at Reynolds number between 30 and 5000, using extended self-similarity *Europhys. Lett.* **34**, 411–416.

Bacry, E., Arneodo, A., Frisch, U., Gagne, Y. & Hopfinger, E. 1989 Wavelet analysis of fully developed turbulence data and measurement of the scaling exponents. In *Proc. Turbulence 89: Organized Structures and Turbulence in Fluid Mechanics, Grenoble (France)*, (ed. M. Lesieur & O. Metais), pp. 203–215. Kluwer.

Batchelor G. K. & Townsend A. A. 1949 The nature of turbulent motion at large wavenumbers. *Proc. R. Soc. Lond.* A**199**, 238–255.

Benzi, R., Biferale, L., Ciliberto, S., Struglia, M. V. & Tripiccione, L. 1996 Generalized scaling in fully developed turbulence. *Physica* D **96**, 162–169.

Benzi, R., Ciliberto, S., Baudet, C., Chavarria, G. R. & Tripiccione, R. 1993*a* Extended self-similarity in the dissipation range. *Europhys. Lett.* **24**, 275–279.

Benzi, R., Ciliberto, S., Tripiccione, R., Baudet, C., Massaioli, F. & Succi, S. 1993*b* Extended self-similarity in turbulent flows. *Phys. Rev.* E **48**, 29–32.

Benzi, R., Ciliberto, S. & Chavarria, G. R. 1995 On the scaling of three dimensional homogeneous and isotropic turbulence. *Physica* D **80**, 385–398.

Biferale, L. 1992 Leggi di scala anomale nella turbolenza sviluppata. PhD thesis, University "La Sapienza", Rome, Italy.

Briscolini, M. & Santangelo, P. 1994 The non-Gaussian statistics of the velocity field in low-resolution large-eddy simulations of homogeneous turbulence. *J. Fluid Mech.* **270**, 94–122.

Cadot, O., Douady, S. & Couder, Y. 1995 Characterization of the low pressure filaments in a 3D turbulent shear flow. *Phys. Fluids* **7**, 630–634.

Camussi, R., Barbagallo, D., Guj, G. & Stella, F. 1996*a* Transverse and longitudinal scaling laws in non-homogeneous low *Re* turbulence. *Phys. Fluids* **8**, 1181–1191.

Camussi, R., Ciliberto, S., Benzi, R. & Baudet, C. 1996*b* Statistical uncertainty of turbulence measurements. *Phys. Rev.* E **54**, 100–102.

Camussi, R., Ciliberto, S., Benzi, R. & Baudet, C. 1996*c* The scaling of the velocity increments correlation function. *Phys. Fluids* **8**, 1686–1688.

Camussi, R. & Guj, G. 1996 Experimental analysis of scaling laws in low Re_λ grid-generated turbulence. *Exps. Fluids* **20**, 199–209.

Castaing, B., Gagne, Y. & Hopfinger, E. J 1990 Velocity probability density functions of high Reynolds number turbulence. *Physica* D **46**, 177–200.

Daubechies, I. 1992 *Ten Lectures on Wavelets.* CBMS-NSF Reg. Conf. Ser. Appl. Maths.

Douady, S., Couder, Y. & Brachet, P. 1991 Direct observation of the intermittency of intense vorticity filaments in turbulence. *Phys. Rev. Lett.* **67**, 983–986.

FARGE, M. 1992 Wavelet transforms and their applications to turbulence. *Ann. Rev. Fluid Mech.* **24**, 395–457.

GAGNE, Y. 1987 Etude expérimentale de l'intermittence et des singularités dans le plan complexe en turbulence développée. PhD Thesis, University of Grenoble.

HINZE, J. O. 1975 *Turbulence*, *2nd edn.* McGraw-Hill.

JIMÉNEZ, J., WRAY, A. A., SAFFMAN, P. G. & ROGALLO, R. S. 1993 The structure of intense vorticity in isotropic turbulence. *J. Fluid Mech.* **255**, 65–90.

KERR, R. 1985 Higher order derivative correlations and the alignment of small scale structures in isotropic numerical turbulence. *J. Fluid Mech.* **153**, 31–58.

KEVLAHAN, N. K. R. & VASSILICOS, J. C. 1994 The space and scale dependencies of the self-similar structure of turbulence. *Proc. R. Soc. Lond.* A **447**, 238–255.

KOLMOGOROV, A. 1941 The local structure of turbulence in incompressible viscous fluid for very large Reynolds numbers. *C. R. Akad. Sci. SSSR* **30**, 301–305.

KOLMOGOROV, A. 1962 A refinement of previous hypotheses concerning the local structure of turbulence in viscous incompressible fluid at high Reynolds number. *J. Fluid Mech.* **13**, 82–85.

KUO, A. Y. S. & CORRSIN, S. 1972 Experiments on the geometry of the fine-structure regions in fully turbulent fluid. *J. Fluid Mech.* **56**, 447–479.

MALLAT, S. 1989, A theory for multiresolution signal decomposition: the wavelet representation. *IEEE Trans. PAMI* **11** 674–693 (Table 1).

MENEVEAU, C. 1991*a* Analysis of turbulence in the orthonormal wavelet representation. *J. Fluid Mech.* **232**, 469–520.

MENEVEAU, C. 1991*b* Appendices A,B and C to CTR manuscript 120 CTR Summer Prog.

MENEVEAU, C. & SREENIVASAN, K. R. 1991 The multifractal nature of turbulent energy dissipation. *J. Fluid Mech.* **224**, 429–484.

MIMOUNI, S., LAVAL, G., SCHEURER, B. & JAFFARD, S. 1995 Morphology of the mixing layer in the Rayleigh–Taylor instability. In *Small-Scale Structures in Three Dimensional Hydrodynamic and Magneto-Hydrodynamic Turbulence.* (ed. V Meneguzzi & A. Pouquet). Lecture Notes in Physics. pp. 179–192. Springer.

MONIN, A. S. & YAGLOM, A. M. 1975 *Statistical Fluid Mechanics*, vol. 2. MIT Press.

OBOUKOV, A. M. 1962 Some specific features of atmospheric turbulence. *J. Fluid Mech.* **13**, 77–81.

SHE, Z.-S. 1991 Intermittency and non-Gaussian statistics in turbulence. *Fluid Dyn. Res.* **8**, 143–158.

SHE, Z.-S. & LEVESQUE, E. 1994 Universal scaling laws in fully developed turbulence. *Phys. Rev. Lett.* **72**, 336–338.

SHE, Z.-S., JACKSON, E. & ORSZAG, S. A. 1988 Scale dependent intermittency and coherence in turbulence. *J. Sci. Comput.* **3**, 407–410.

SHE, Z.-S., JACKSON, E. & ORSZAG, S. A. 1991 Intermittent vortex structures in homogeneous isotropic turbulence. *Nature* **144**, 226–228.

VASSILICOS, J. C. 1996 Topological classification and identification of small-scale turbulence structures. In *Eddy Structure Identification* (ed. J. P. Bonnet), Springer.

VILLERMEAUX, E., SIXOU, B. & GAGNE, Y. 1995 Intense vortical structures in grid-generated turbulence. *Phys. Fluids* **7**, 2008–2013.

VINCENT, A. & MENEGUZZI, M. 1991 The spatial structure and statistical properties of homogeneous turbulence. *J. Fluid Mech.* **225**, 1–25.